Supporting Information

High Toughness Multifunctional Organic Hydrogels for Flexible Strain and Temperature Sensor

Hongjie Chen [a,b,⊥], *Jianren Huang,* [a,b,⊥] *Jiantao Liu,* [a] *Jianfeng Gu,* [c] *Jundong Zhu,* [b] *Bing Huang,* [b] *Jin Bai,* [b] *Jinquan Guo,* [a] *Xiaoxiang Yang,* [a]*, *Lunhui Guan* [b]*

a. School of Mechanical Engineering and Automation, Fuzhou University, Fuzhou 350108, People's Republic of China

b. CAS Key Laboratory of Design and Assembly of Functional Nanostructures, Fujian Key Laboratory of Nanomaterials, Fujian Institute of Research on the Structure of Matter, Chinese Academy of Sciences, Fuzhou 350002, China.

c. College of Chemical Engineering, Fuzhou University, Fuzhou 350108, People's Republic of China

⊥.Authors with equal contributions.

*. Corresponding Aauthor

Prof. Xiaoxiang Yang Email: yangxx@fzu.edu.cn

Prof. Lunhui Guan E-mail: guanlh@fjirsm.ac.cn

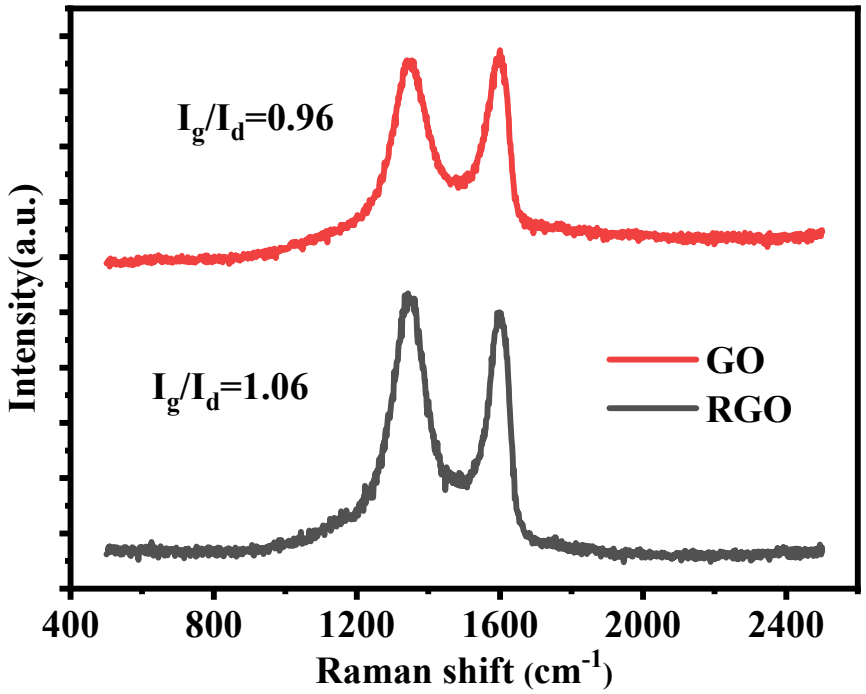

Figure S1. Raman patterns of RGO and GO.

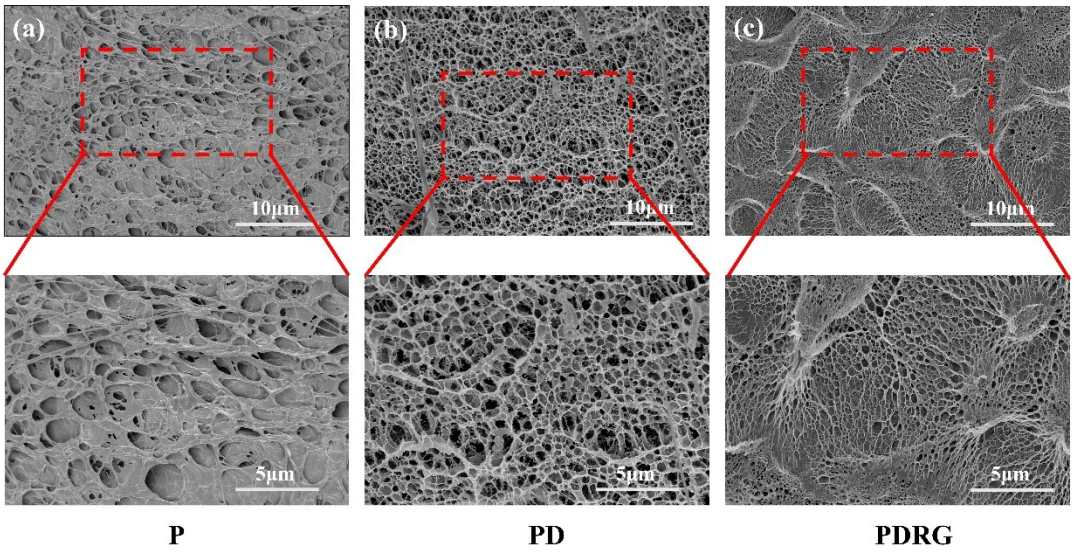

Figure S2. SEM images of (a) P hydrogel (b) PD hydrogel, and (c) PDRG hydrogel

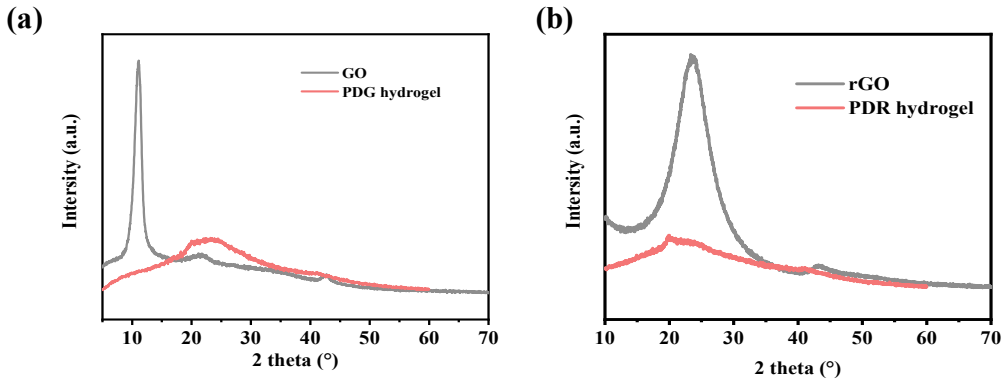

Figure S3. XRD patterns of (a)GO and PDG hydrogel. (b)rGO and PDR hydrogel

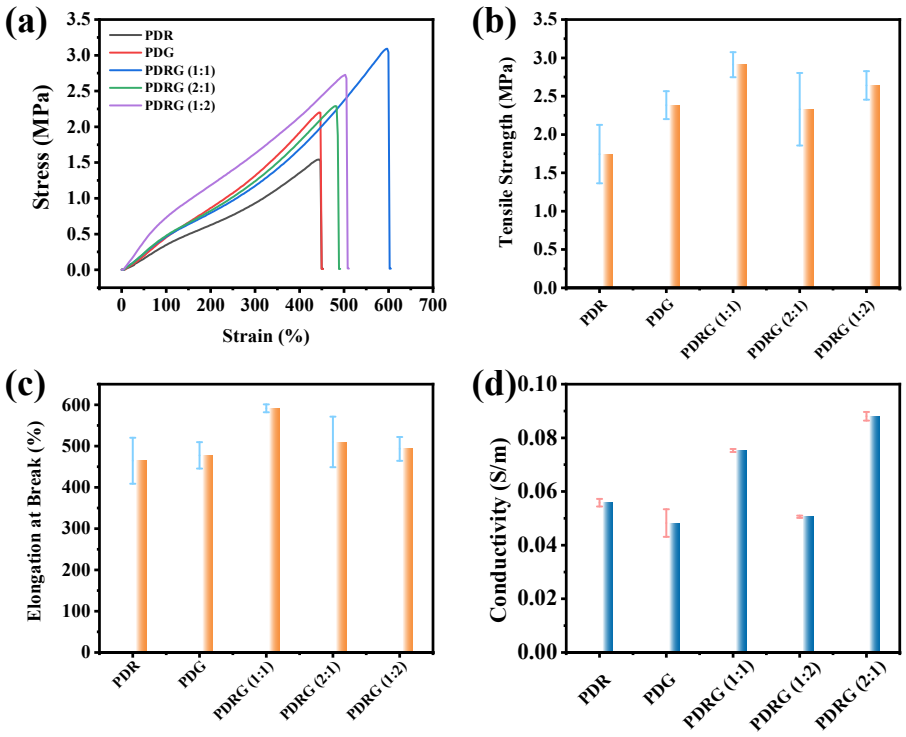

Figure S4. Mechanical and electrical properties of PVA/DMSO/RGO/GO organohydrogels with different ratios of RGO and GO. a) Tensile stress-strain curves ; b) Tensile strength ; c) Elongation at break.and d) conductivity.

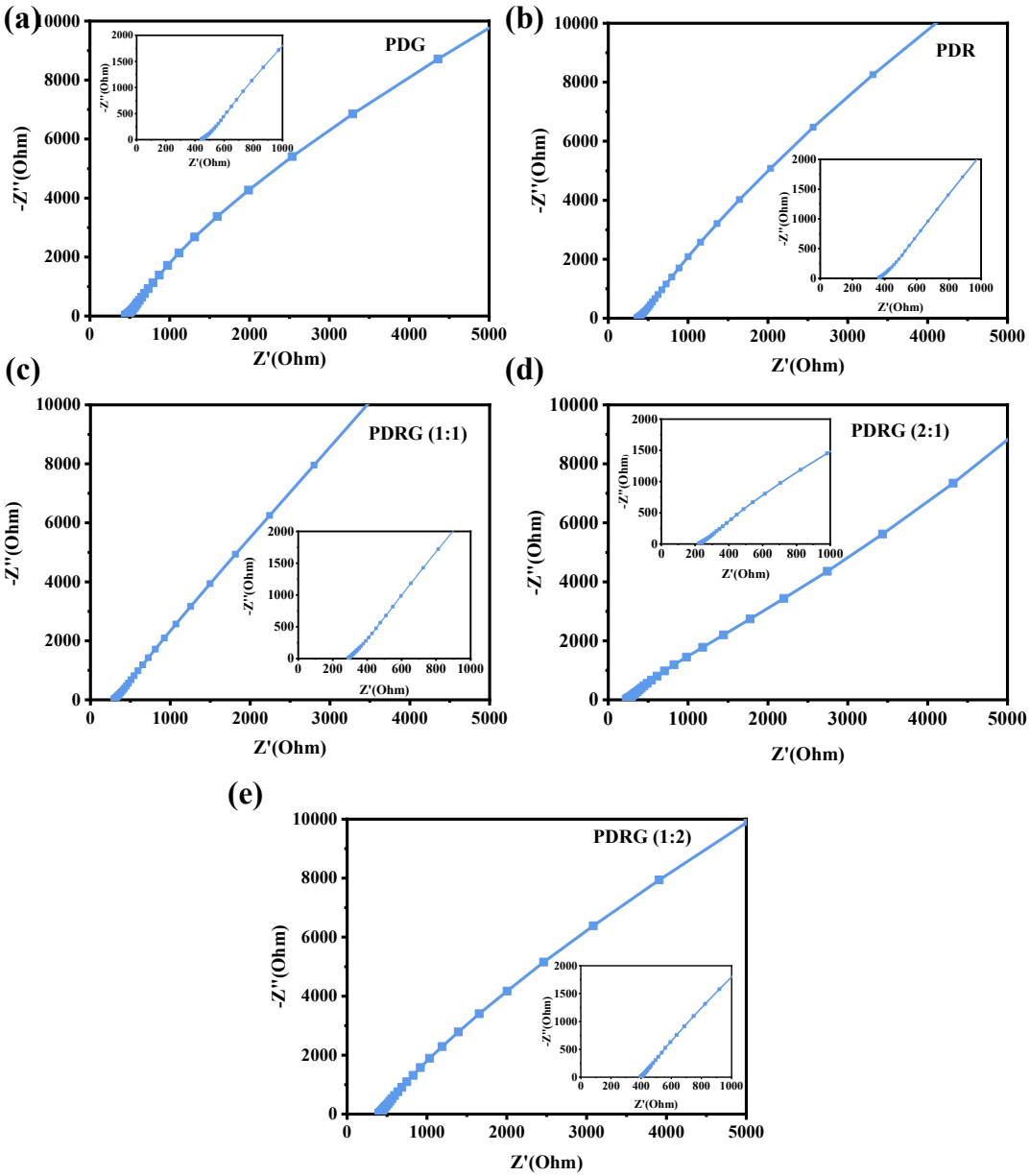

Figure S5. Nyquist impedance plots of the (a) PDG, (b) PDR, (c) PDRG (1:1), (d) PDRG (2:1), (e) PDRG (1:2) organohydrogels

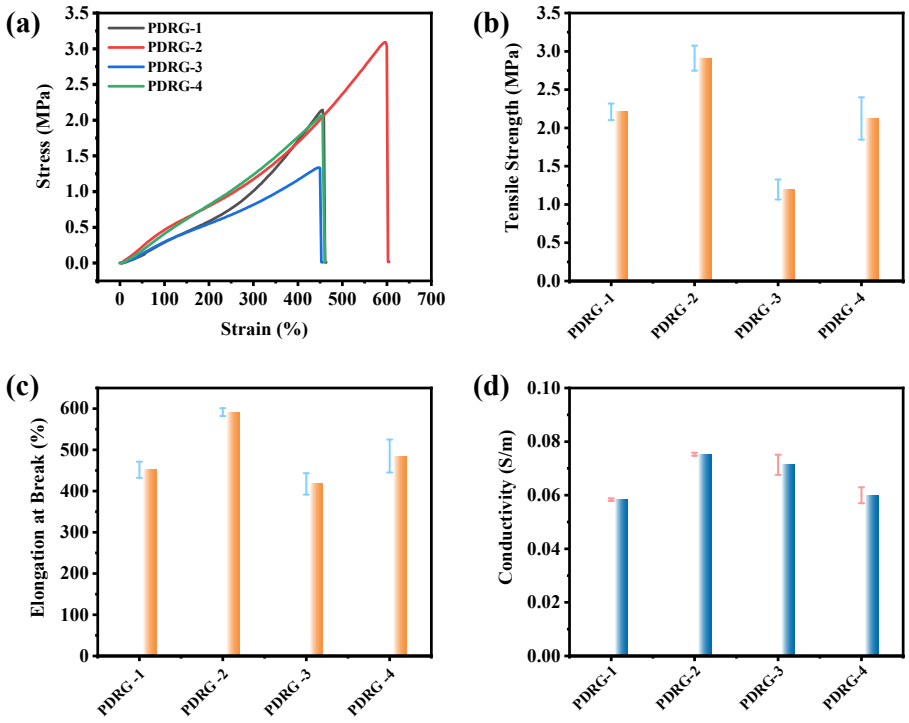

Figure S6. Mechanical and electrical properties of PVA/DMSO/RGO/GO organohydrogel with different content of total RGO and GO addition: a) Tensile stress-strain curves; b) Tensile strength; c) Elongation at break and d) conductivity.

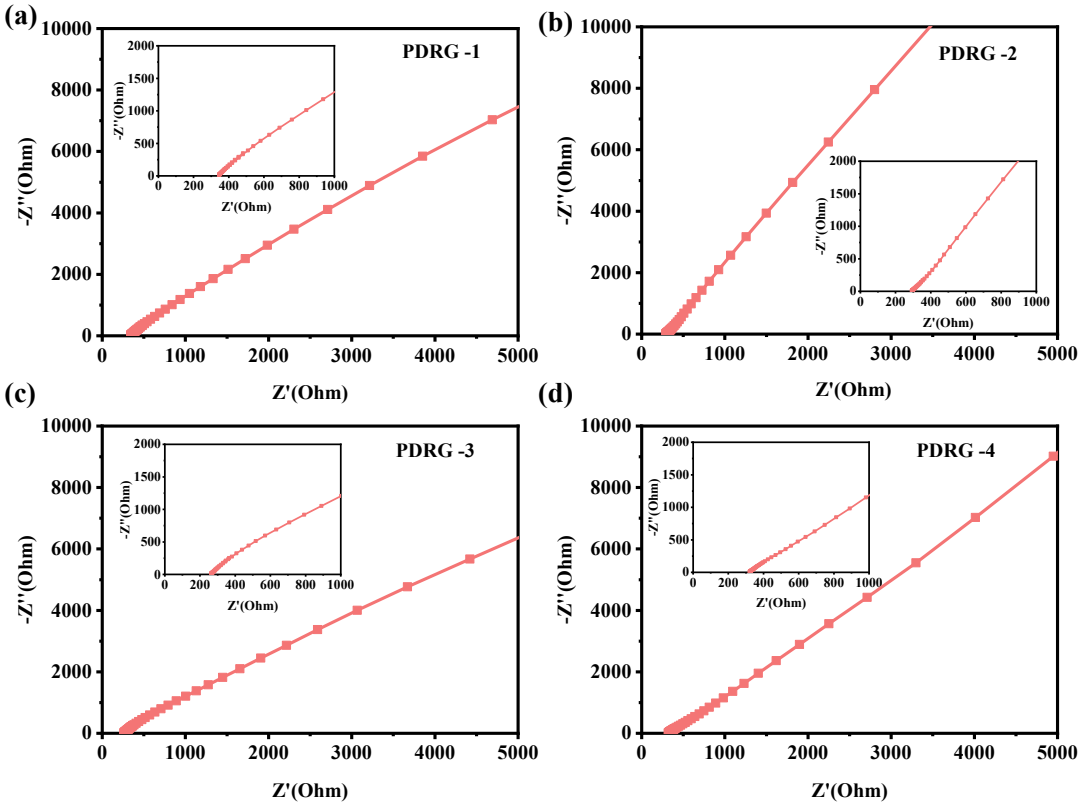

Figure S7. Nyquist impedance plots of the PVA/DMSO/RGO/GO organohydrogel with different content of total RGO and GO addition (a) PDRG-1,(b) PDRG-2,(c) PDRG-3,(d) PDRG-4 .

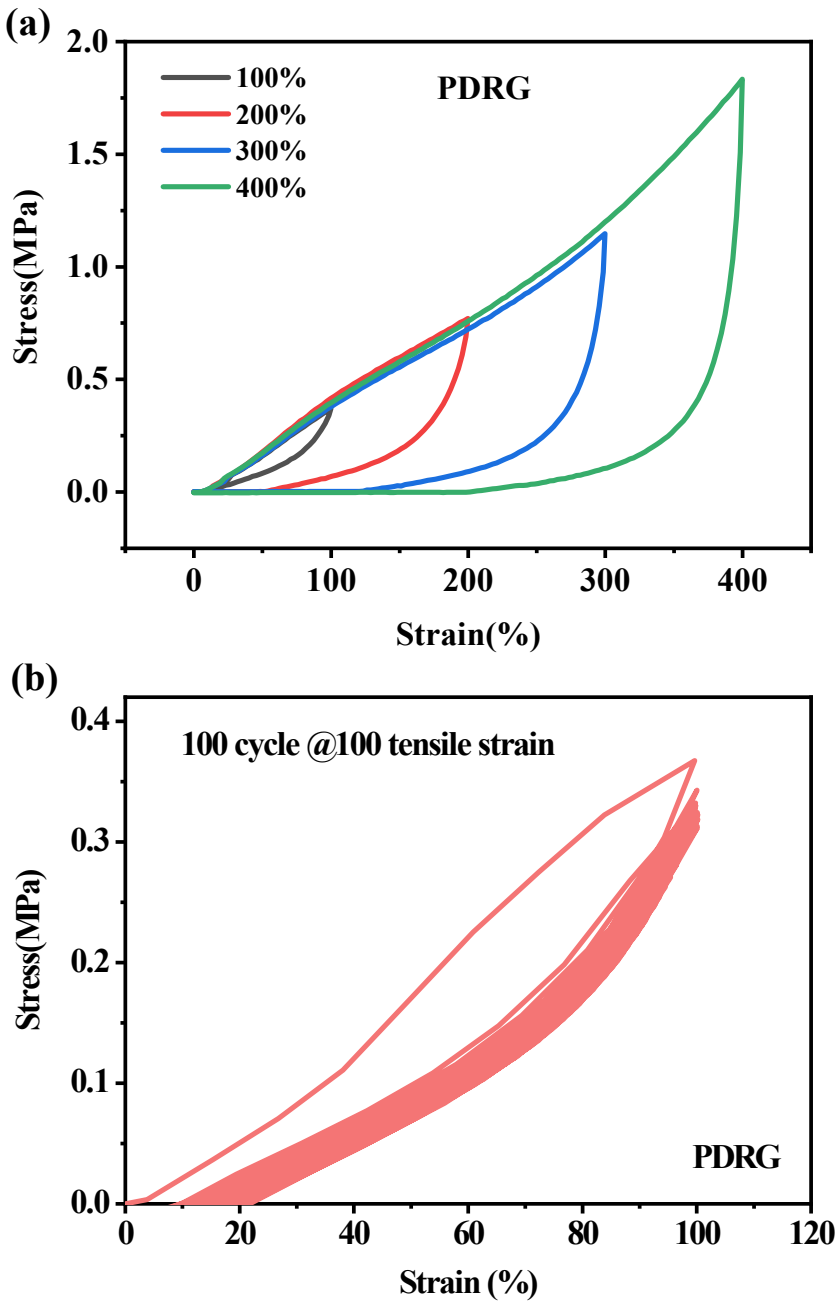

Figure S8. (a) loading−unloading cycle behaviors of the as-prepared organohydrogel; (b) loading−unloading measurement of the PDRG organohydrogel under varied strains without a resting interval.

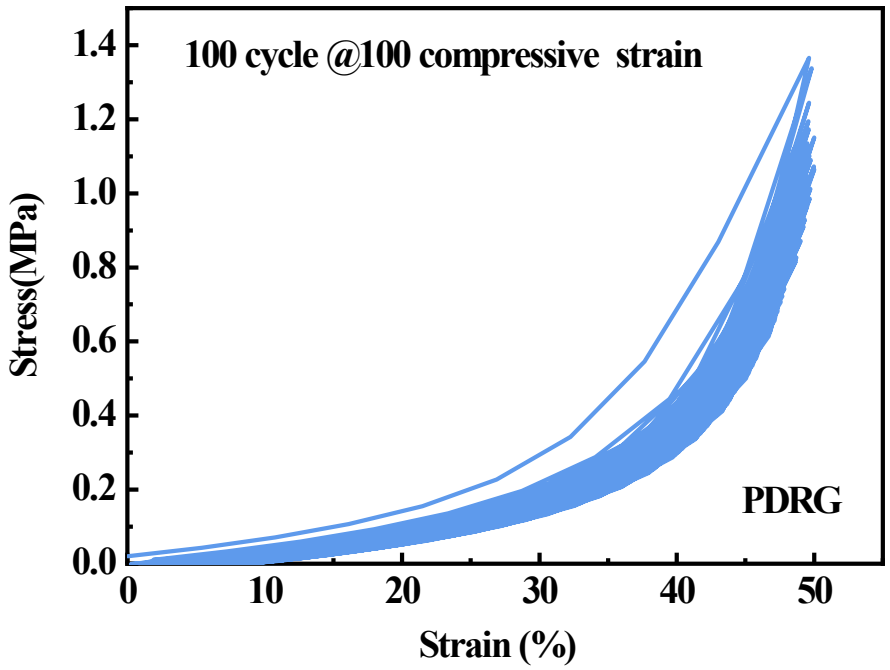

Figure S9. 50% compressive strain without resting time between two consecutive tests.

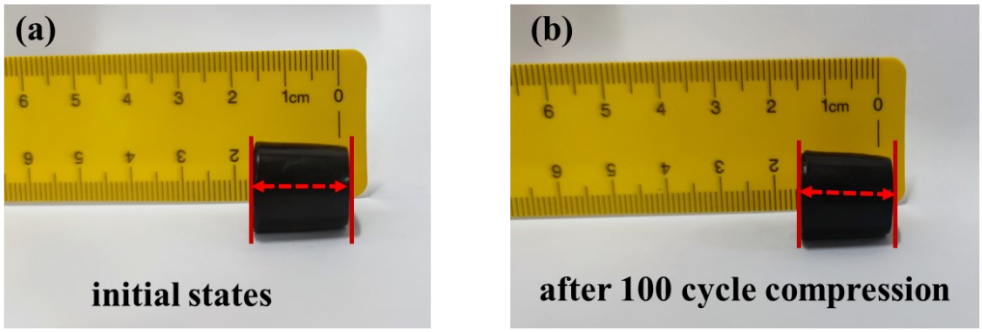

Figure S10. The organohydrogel a) before compression and b) after 100 cycle compression.

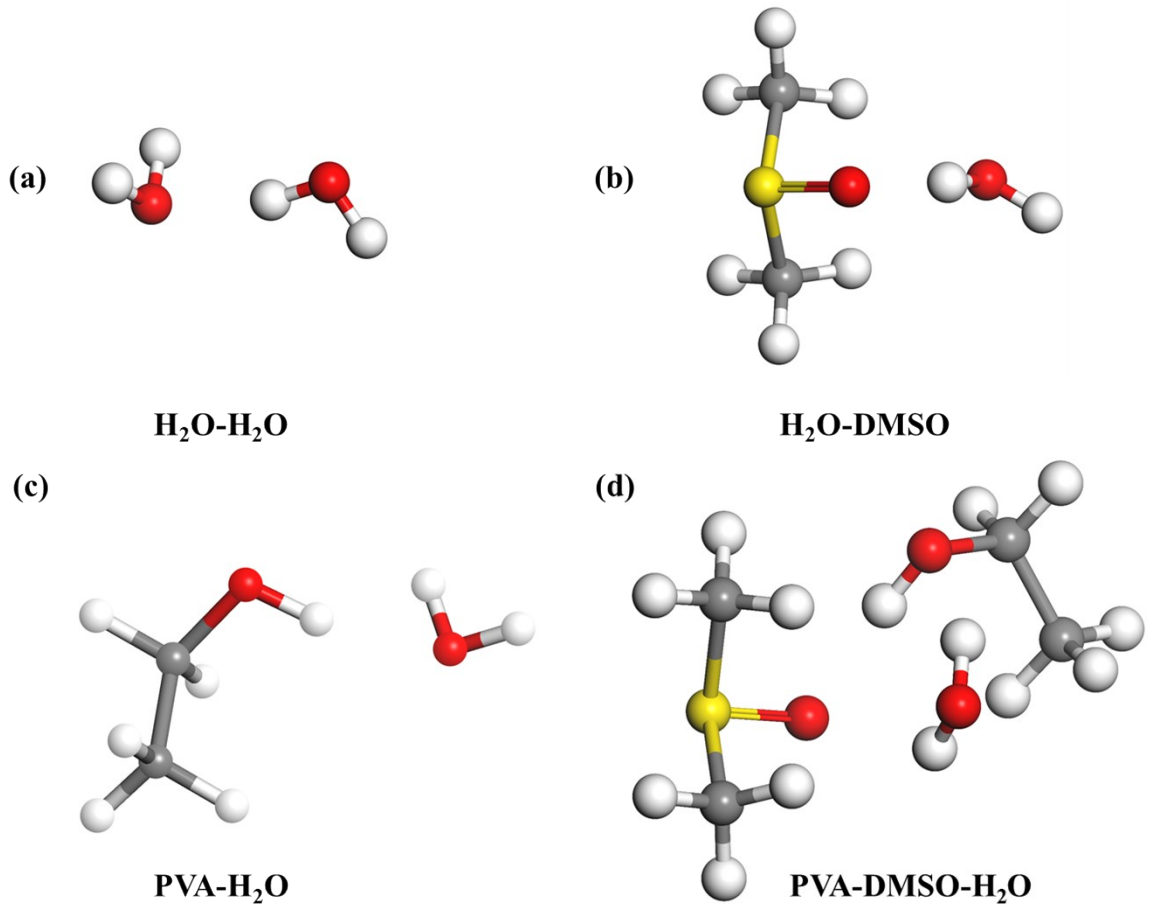

Figure S11. DFT analysis and hydrogen bonding interactions of (a)H2O-H2O, (b) DMSO-H2O, (c) PVA-DMSO-H2O, (d) PVA-DMSO-H2O.

To investigate the intermolecular interactions between PVA, DMSO, and H_2O, density functional theory (DFT) calculations were conducted by Dmol3 module in Materials Studio software package.[1] The geometry optimizations were performed using the Perdew-Burke-Ernzerh of (PBE)[2] modification of the generalized gradient approximation (GGA)[3] with the Grimme[4,5] custom method for DFT-D correction together with the doubled numerical basis set plus polarization basis sets (DNP,including polarization d- function), and the cutoff energy for the plane-wave basis set is set to be 240.0 eV while the k-point is set to 7×7×1 to achieve high accuracy. The core electrons were treated by the DFT semi-core pseudo potentials, and a global orbital cutoff of 3.2 Å and a Fermi smearing of 0.005 Ha were used for the simulations. The convergence criteria including self-consistent field (SCF) tolerance of 1.0×10^{-5} Ha

per atom, a maximum force tolerance of 0.002 Ha Å-1, an energy tolerance of 1.0×10^{-5} Ha per atom and a maximum displacement tolerance of 0.005 Å were employed. The interaction energy (ΔEint) is the difference between the total energy of the complex and the sum of total energies of its components.

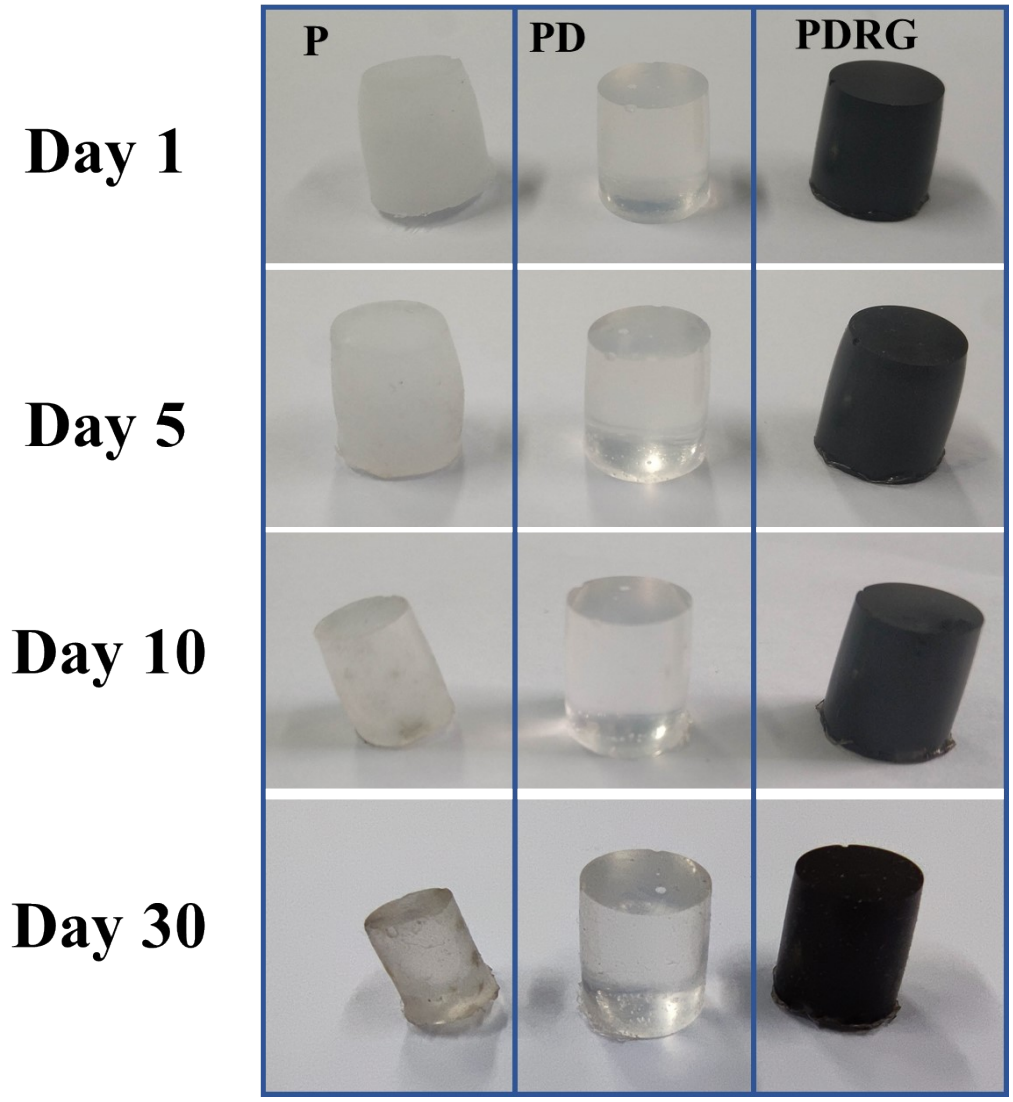

Figure S12. Topography change of the P hydrogel, PD and PDRG organohydrogels**.**

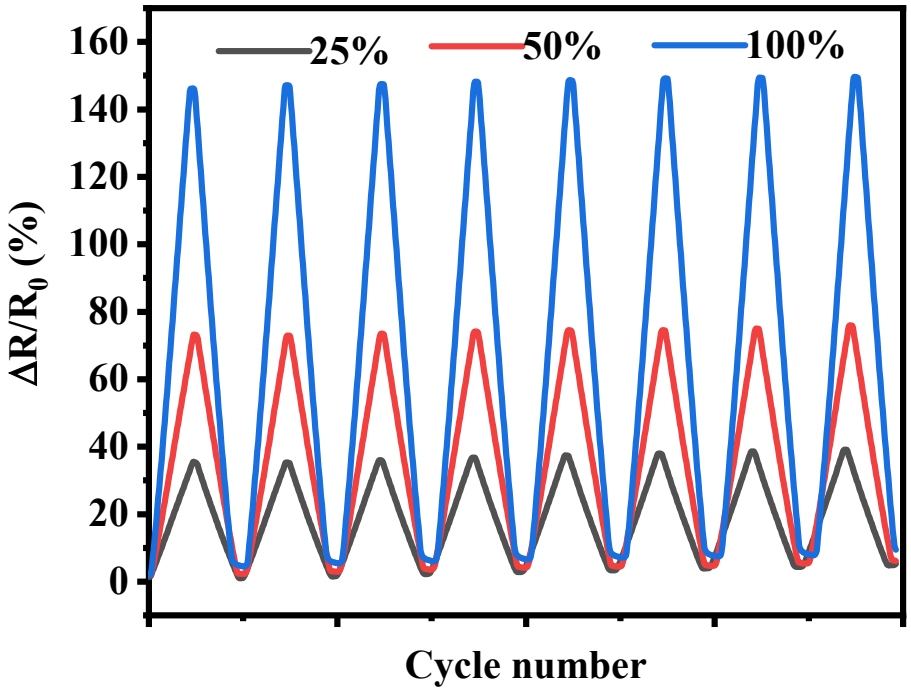

Figure S13. Relative resistance variation of the sensor for a large strain (25%、50%、100%)

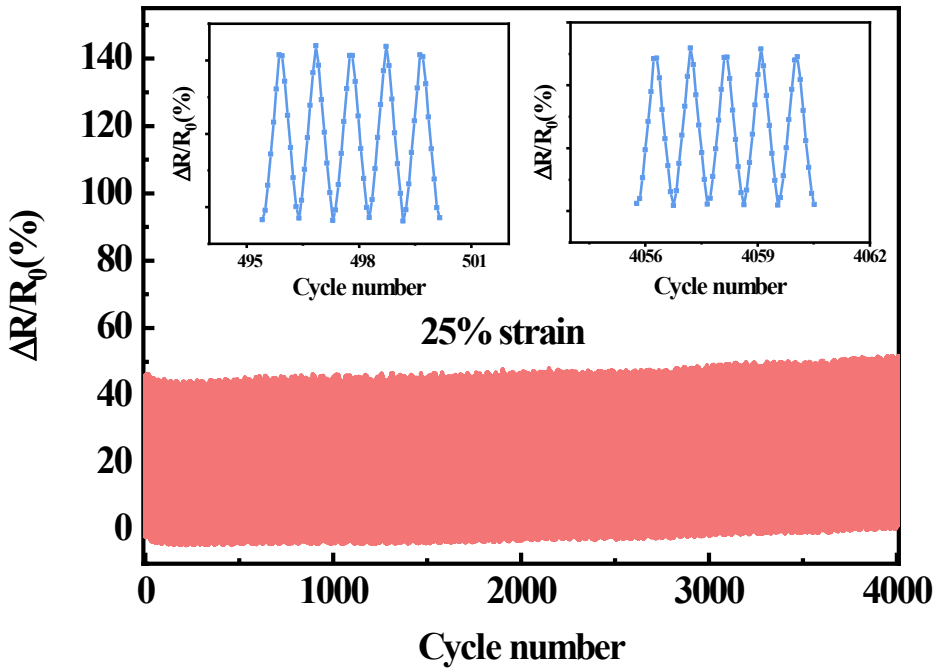

Figure S14. Relative resistance response under repeated loading−unloading at 25% tensile strain for 4000 cycles. Magnified signal during 495−501 and 4056−4062 cycles.

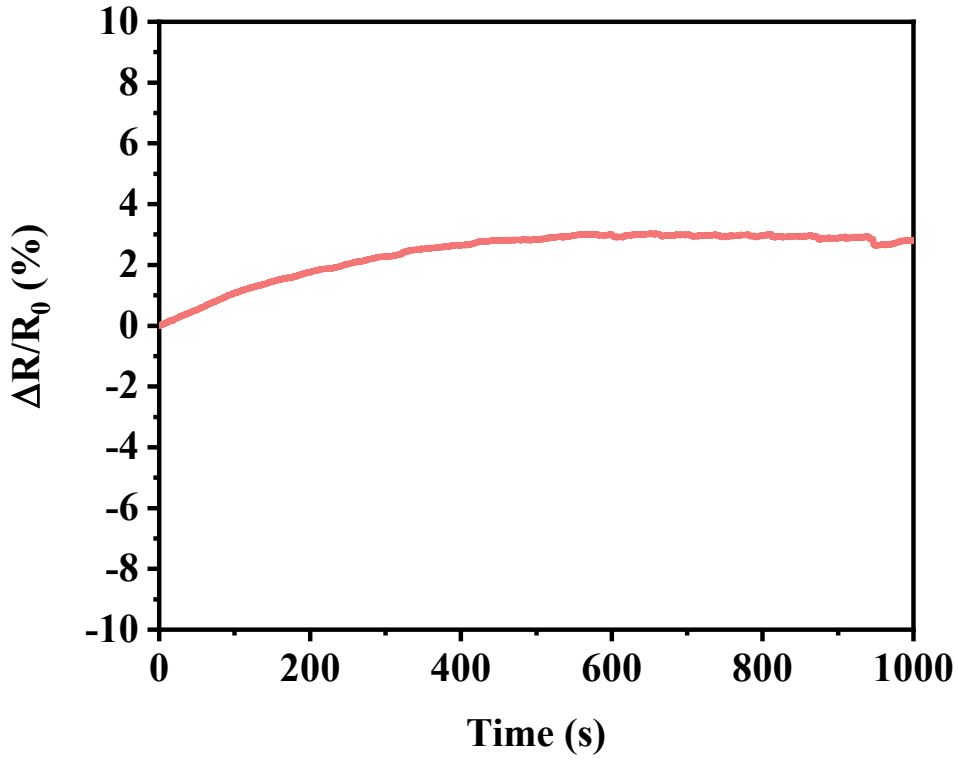

Figure S15. Relative resistance variation of hydrogel sensor stored at -30 °C.

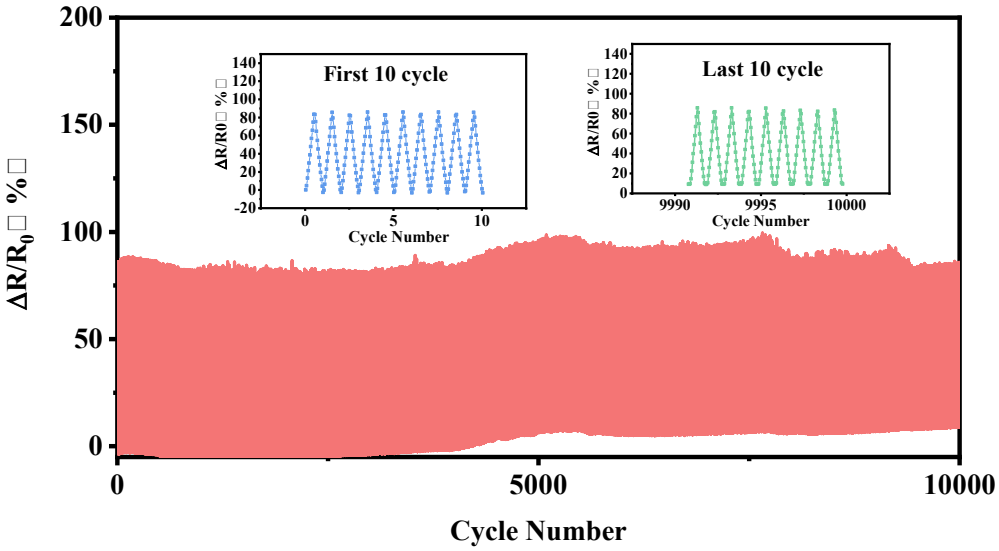

Figure S16. The sensing response of the PDRG sensor after being storage at open environment for 7 days towards 10000 cyclic loadings at 50% strain.

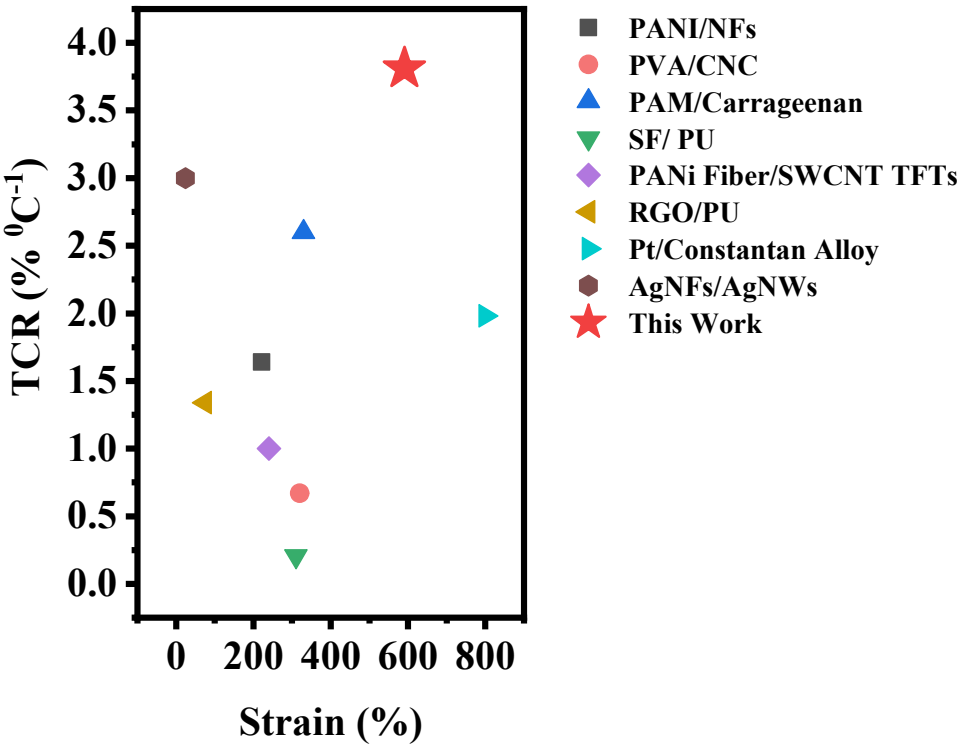

Figure S17. Comparison of performance parameters with various flexible temperature sensors reported in the literature.

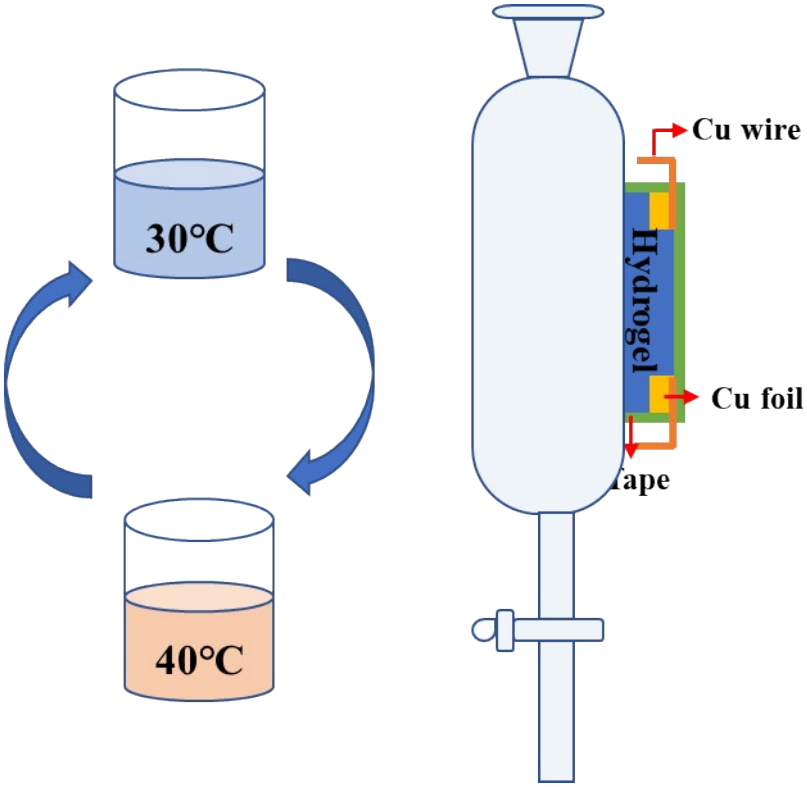

Figure S18. Schematic diagram of response to different temperatures of water

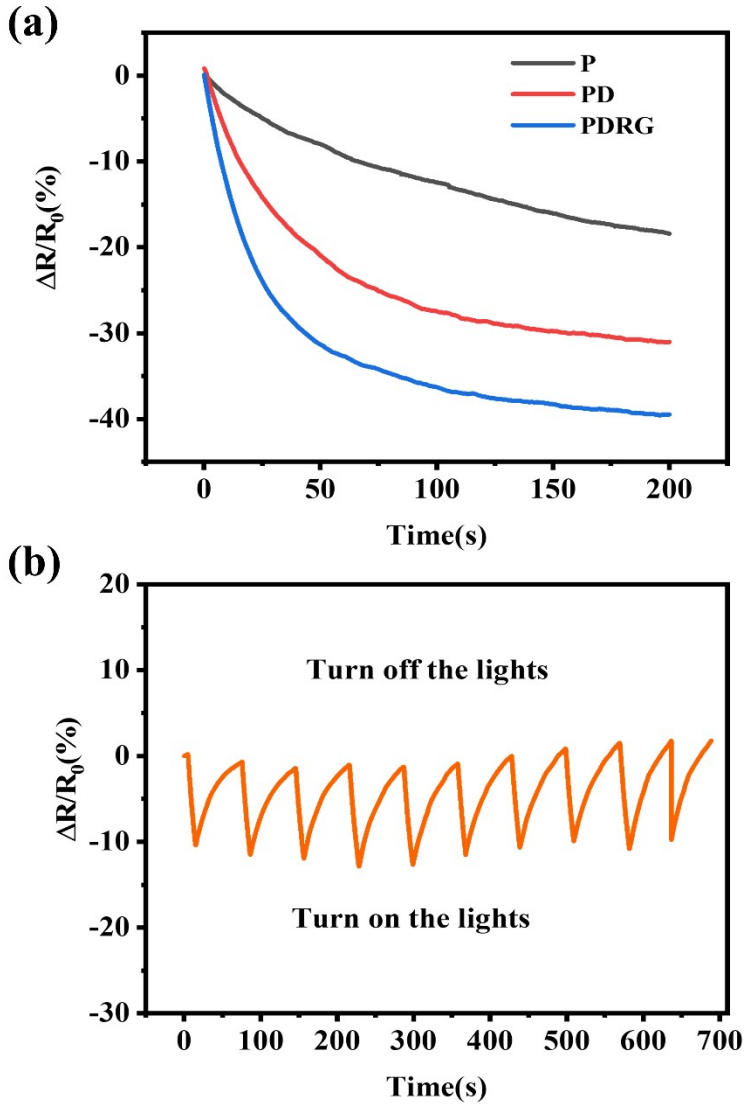

Figure S19. The photothermal performance of PDRG organohydrogel sensor: (a) resistance change of different gels under infrared irradiation (b) resistance change of 10s infrared irradiation and 60s recovery time.

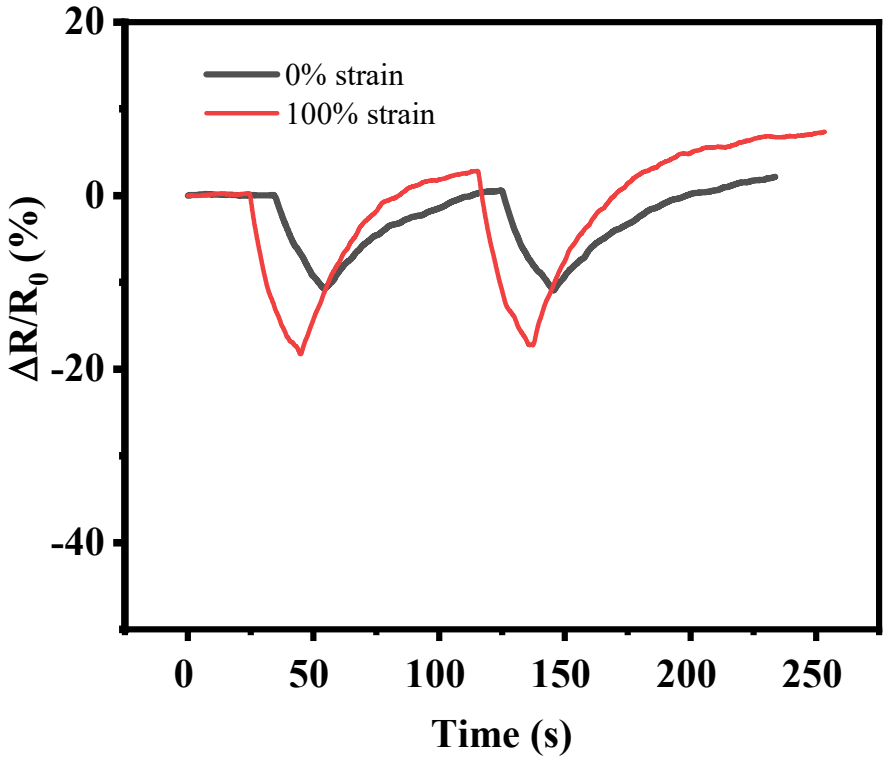

Figure S20. Resistance change of different strain under infrared irradiation

Table S1. The experimental ingredients and nomenclatures of as-prepared hydrogel and organohydrogels.

Sample	PVA (g)	GO(g)	RGO(g)	Water (mL)	DMSO (g)
P	1.6	0	0	9	0
PD	1.6	0	0	6	3
PDG	1.6	0.009	0	6	3
PDR	1.6	0	0.009	6	3
PDRG(RGO:GO=1:1)	1.6	0.0045	0.0045	6	3
PDRG(RGO:GO=1:2)	1.6	0.006	0.003	6	3
PDRG(RGO:GO=2:1)	1.6	0.003	0.006	6	3
PDRG-1	1.6	0.0015	0.0015	6	3
PDRG-2	1.6	0.0045	0.0045	6	3
PDRG-3	1.6	0.0075	0.0075	6	3
PDRG-4	1.6	0.0105	0.0105	6	3

Table S2. The mass percentage of each component for the samples in this work.

Sample	PVA (wt%)	DMSO(wt%)	GOwt‰)	RGO (wt‰)	GO+RGO (wt‰)	Water (wt%)
P	15.09	0.00	0.00	0.00	0.00	84.91
PG	15.09	28.30	0.00	0.00	0.00	56.61
PDG	15.08	28.28	0.848	0	0.848	56.55
PDR	15.08	28.28	0	0.848	0.848	56.55
PDRG(RGO:GO=1:1)	15.08	28.28	0.424	0.424	0.848	56.55
PDRG(RGO:GO=1:2)	15.08	28.28	0.564	0.282	0.848	56.55
PDRG(RGO:GO=2:1)	15.08	28.28	0.282	0.564	0.848	56.55
PDRG-1	15.09	28.29	0.141	0.141	0.282	56.59
PDRG-2	15.08	28.28	0.424	0.424	0.848	56.55
PDRG-3	15.07	28.26	0.706	0.706	1.412	56.53
PDRG-4	15.06	28.25	0.989	0.989	1.977	56.50

Table S3. DFT calculation results of the interaction energy of the different systems.

Model	**Interaction energy (eV)**	**Interaction energy (kcal/mol)**
$H_2O…H_2O$	-0.311	-7.172
DMSO…H2O	-0.611	-14.089
PVA…DMSO…H2O	-1.293	-29.817
PVA…H_2O	-0.326	-7.529

Table S4. Comparison of the properties of PVA/DMSO/rGO/GO organohydrogel sensor with other reported flexible hydrogel-based strain sensors.

Materials	Strain at break (%)	Tensile strength (MPa)	Low-temperature tolerant	Gauge factor	Reference
PDRG	591	2.91	√	2.1	This Work
HPC/PVA	975	1.3	×	0.984	[1]
PANi/PA/PVA	160	0.120	×	1.43	[2]
Cellulose/ chitin/ chitosan	129	0.021	√	0.3	[3]
PAAm-oxCNTs	700	0.71	×	3.39	[4]
HK/PVA/NaCl	620	1.36	×	4.92	[5]
Alginate–gelatin/$CaCl_2$	310	0.012	√	1.86	[6]
PANI/PSS/UPy	700	0.01	×	3.4	[7]
PAN/DMF	800	0.56	×	~	[8]
PVA-G-PDA-AgNPs	331	1.174	×	0.93	[9]
sG / PVA	0.213	0.245	×	~	[10]
HAPAAm/CNTs	3000	0.050	×	4.32	[11]
PAA/PVA/F-MWCNT	550%	0.025	√	0.71	[12]
HAPAM/CNCs@CNTs	2900%	0.2	×	7.63	[13]
PAAM/PVP/EG /GO	10500%	0.037	×	0.8	[14]
PAM/SF/GO/PEDOT:PSS	600%	0.119	×	1.6	[15]
PAA/GO	700%	0.348	×	1.32	[16]

Table S5. Comparison of the properties of PVA/DMSO/rGO/GO organohydrogel senor with other reported flexible hydrogel-based temperature sensors.

Materials	Temperature coefficient of resistance(%$^{o}C^{-1}$)	Strain at break (%)	Tensile strength (MPa)	Sensing ranges(^{o}C)	Reference
PDRG	3.81	591	2.91	20-85	This Work
PANI/NFs	1.64	221.8	0.519	40-110	[17]
PVA/CNC	0. 67	320	0.421	15-45	[18]
PANI-HNSs	8.1			25-100	[19]
PAM/carrageenan	2.6	330		22-92	[20]
SF/polyurethane	0.205	310	12	20-160	[21]
Aligned carbon nanofiber	1.52			30-55	[22]
PANI nanofiber/SWCNT TFTs	1	240		15-45	[23]
RGO/PU	1.34	75		30-80	[24]
platinum (Pt) and constantan alloy (45% Ni, 55% Cu)	1.98	800		27-71	[25]
AgNFs/AgNWs	3	24.11		30-45	[26]
Ag nanocrystal/PDMS	0.185			30-50	[27]

References

1 Y. Zhou, C. Wan, Y. Yang, H. Yang, S. Wang, Z. Dai, K. Ji, H. Jiang, X. Chen and Y. Long, *Adv. Funct. Mater.*, , DOI:10.1002/adfm.201806220.

2 Y. Zhao, B. Zhang, B. Yao, Y. Qiu, Z. Peng, Y. Zhang, Y. Alsaid, I. Frenkel, K. Youssef, Q. Pei and X. He, *Matter*, 2020, **3**, 1196–1210.

3 R. Tong, G. Chen, D. Pan, H. Qi, R. Li, J. Tian, F. Lu and M. He, *Biomacromolecules*, 2019, **20**, 2096–2104.

4 X. Sun, Z. Qin, L. Ye, H. Zhang, Q. Yu, X. Wu, J. Li and F. Yao, *Chem. Eng. J.*, 2020, **382**, 122832.

5 Y. Gao, S. Gu, F. Jia and G. Gao, *J. Mater. Chem. A*, 2020, **8**, 24175–24183.

6 X. Zhang, K. Wang, J. Hu, Y. Zhang, Y. Dai and F. Xia, *J. Mater. Chem. A*, 2020, **8**, 25390–25401.

7 J. Chen, Q. Peng, T. Thundat and H. Zeng, *Chem. Mater.*, 2019, **31**, 4553–4563.

8 X. Guo, C. Zhang, L. Shi, Q. Zhang and H. Zhu, *J. Mater. Chem. A*, 2020, **8**, 20346–20353.

9 L. Fan, J. Xie, Y. Zheng, D. Wei, D. Yao, J. Zhang and T. Zhang, *ACS Appl. Mater. Interfaces*, 2020, **12**, 22225–22236.

10 W. Yao, C. Geng, D. Han, F. Chen and Q. Fu, *RSC Adv.*, 2014, **4**, 39588–39595.

11 Z. Qin, X. Sun, Q. Yu, H. Zhang, X. Wu, M. Yao, W. Liu, F. Yao and J. Li, *ACS Appl. Mater. Interfaces*, 2020, **12**, 4944–4953.

12 G. Ge, W. Yuan, W. Zhao, Y. Lu, Y. Zhang, W. Wang, P. Chen, W. Huang, W. Si and X. Dong, *J. Mater. Chem. A*, 2019, **7**, 5949–5956.

13 G. Su, J. Cao, X. Zhang, Y. Zhang, S. Yin, L. Jia, Q. Guo, X. Zhang, J. Zhang and T. Zhou, *J. Mater. Chem. A*, 2020, **8**, 2074–2082.

14 H. Zhang, W. Niu and S. Zhang, *ACS Appl. Mater. Interfaces*, 2018, **10**, 32640–32648.

15 F. He, X. You, H. Gong, Y. Yang, T. Bai, W. Wang, W. Guo, X. Liu and M. Ye, *ACS Appl. Mater. Interfaces*, 2020, **12**, 6442–6450.

16 X. Jing, H. Y. Mi, X. F. Peng and L. S. Turng, *Carbon N. Y.*, 2018, **136**, 63–72.

17 G. Ge, Y. Lu, X. Qu, W. Zhao, Y. Ren, W. Wang, Q. Wang, W. Huang and X. Dong, *ACS Nano*, 2019, acsnano.9b07874.

18 J. W. Kim, H. Park, G. Lee, Y. R. Jeong, S. Y. Hong, K. Keum, J. Yoon, M. S. Kim and J. S. Ha, *Adv. Funct. Mater.*, 2019, **29**, 1–14.

19 Z. Lou, S. Chen, L. Wang, R. Shi, L. Li, K. Jiang, D. Chen and G. Shen, *Nano Energy*, 2017, **38**, 28–35.

20 J. Wu, S. Han, T. Yang, Z. Li, Z. Wu, X. Gui, K. Tao, J. Miao, L. K. Norford, C. Liu and F. Huo, *ACS Appl. Mater. Interfaces*, 2018, **10**, 19097–19105.

21 J. Huang, Z. Xu, W. Qiu, F. Chen, Z. Meng, C. Hou, W. Guo and X. Y. Liu, *Adv. Funct. Mater.*, 2020, **30**, 1–9.

22 J. H. Lee, H. Chen, E. Kim, H. Zhang, K. Wu, H. Zhang, X. Shen, Q. Zheng, J. Yang, S. Jeon and J. K. Kim, *Mater. Horizons*, 2021, **8**, 1488–1498.

23 S. Y. Hong, Y. H. Lee, H. Park, S. W. Jin, Y. R. Jeong, J. Yun, I. You, G. Zi and J. S. Ha, *Adv. Mater.*, 2016, **28**, 930–935.

24 T. Q. Trung, S. Ramasundaram, B. U. Hwang and N. E. Lee, *Adv. Mater.*, 2016, **28**, 502–509.

25 Q. Hua, J. Sun, H. Liu, R. Bao, R. Yu, J. Zhai, C. Pan and Z. L. Wang, *Nat. Commun.*, 2018, **9**, 1–11.

26 B. W. An, S. Heo, S. Ji, F. Bien and J. U. Park, *Nat. Commun.*, 2018, **9**, 1–10.

27 J. Bang, W. S. Lee, B. Park, H. Joh, H. K. Woo, S. Jeon, J. Ahn, C. Jeong, T. il Kim and S. J. Oh, *Adv. Funct. Mater.*, 2019, **29**, 1–8.